EINDHOVEN UNIVERSITY OF TECHNOLOGY

Eindhoven University of Technology

BACHELOR

# Optimization of platinum atomic layer deposition on the FlexAL setup

van Stiphout, T.A.P.

*Award date:*
2013

Link to publication

**Disclaimer**
This document contains a student thesis (bachelor's or master's), as authored by a student at Eindhoven University of Technology. Student theses are made available in the TU/e repository upon obtaining the required degree. The grade received is not published on the document as presented in the repository. The required complexity or quality of research of student theses may vary by program, and the required minimum study period may vary in duration.

**General rights**
Copyright and moral rights for the publications made accessible in the public portal are retained by the authors and/or other copyright owners and it is a condition of accessing publications that users recognise and abide by the legal requirements associated with these rights.

- Users may download and print one copy of any publication from the public portal for the purpose of private study or research.
- You may not further distribute the material or use it for any profit-making activity or commercial gain

Technische Universiteit Eindhoven
University of Technology

Department of Applied Physics
Plasma & Materials Processing

# Optimization of platinum atomic layer deposition on the FlexAL setup

T.A.P. van Stiphout

*November 2013* *PMP 13-12*

Under supervision of:

A.J.M. Mackus
A.A. Bol

## Abstract

Platinum (Pt) is a noble metal with many applications in microelectronics and catalysis. The material can be deposited by atomic layer deposition (ALD), which results in continuous and pinhole-free films with precise thickness control.

Optimization of the ALD process in terms of saturated growth and efficient precursor dosing are of great importance for Pt deposition and are the main goals for this study. In this work, optimizations of the ALD processes are performed for thermal ALD (at 300°C) and plasma ALD (at room temperature) at the FlexAL setup. Therefore, saturation and nucleation curves were measured with spectroscopic ellipsometry (SE) and (time-resolved) optical emission was measured with optical emission spectroscopy (OES).

For the optimization of the thermal ALD process at 300°C, it was found that 8-10 s $MeCpPtMe_3$ dosing and 5 s (300 mTorr) $O_2$ dosing leads to a saturated ALD growth with a growth rate of ~0.49 ± 0.02 Å/cycle which is consistent with results reported for the ALD-I setup (~0.50 ± 0.01 Å/cycle [1]). Process optimization for plasma ALD at room temperate which includes 8 s $MeCpPtMe_3$ dosing, 5 s $O_2$ plasma and 2.5 s $H_2$ plasma exposure, leading to a growth rate of ~0.42 ± 0.02 Å/cycle which also agrees with the ALD-I setup (~0.40 ± 0.04 Å/cycle). Both processes involve relatively high precursor consumption in comparison to the processes characterized on the ALD-I setup. This could be due to the fact that the FlexAL setup has a five times larger surface area where deposition takes place and has therefore a higher precursor consumption than the ALD-I setup. The FlexAL can handle wafers up to 200 mm and has therefore a larger substrate heater than the ALD-I (which can handle wafers up to 100 mm).

Furthermore, from studying the plasma Pt ALD reaction mechanism by OES, it becomes clear that a combustion reaction (with reaction products $H_2O$ and $CO_2$) and a reduction reaction of $PtO_x$ to Pt (with $H_2O$ as reaction product) takes place during the $O_2$ and $H_2$ plasma step, respectively. The reaction product $H_2O$ was dissociated under influence of the plasma exposures into $H_\alpha$ and OH. Consequently, time-resolved OES measurements of $H_\alpha$ and OH are an indication for the occurrence of combustion reactions during the $O_2$ plasma step and reduction reactions during the $H_2$ plasma step. Therefore, OES data have given insight in the reaction products and, the reaction mechanism of Pt deposition. Time-resolved OES data was also used in the optimization of the plasma ALD process.

# Contents

**1 Introduction** **5**
1.1 Atomic layer deposition . . . 5
1.2 Platinum ALD . . . 6
1.3 Aim of this research . . . 7

**2 Experimental Setup** **9**
2.1 FlexAL setup . . . 9
2.2 Platinum ALD . . . 12
2.3 Spectroscopic Ellipsometry . . . 13
2.4 Optical Emission Spectroscopy . . . 14

**3 Results** **16**
3.1 Thermal Pt ALD . . . 16
3.1.1 Saturation of half-reactions . . . 16
3.1.2 Nucleation behavior . . . 17
3.2 Pt plasma ALD at room temperature . . . 20
3.2.1 Process optimization by SE . . . 20
3.2.2 Process optimization by OES . . . 22

**4 Discussion** **25**
4.1 Comparison SE and OES results . . . 25
4.2 Comparison between Pt ALD at FlexAL and ALD-I setups . . . 25

**5 Conclusion** **28**

**6 Outlook** **29**

**References** **30**

**A Appendix** **32**

# 1 Introduction

Ultra-thin films are nowadays used in many areas of modern science and technology. Modern computer chips, for example, are typically built up from a stack of over 20 patterned thin films, fabricated using subsequently executed deposition and patterning processes [2]. The films consist of atomic layers with thickness ranging from less than 1 nm up to several tens of nanometers. Miniaturization in the semiconductor industry has led to the requirement for atomic level control of thin film deposition.

## 1.1 Atomic layer deposition

Atomic layer deposition (ALD) is a thin film deposition technique that is based on alternating self-limiting surface reactions. The advantage of ALD is that it results in continuous and pinhole-free films with precise thickness control and good conformality on 3D structures. Most ALD processes are based on two self-limiting surface reactions. Figure 1.1 illustrates the basic configuration of one ALD cycle which exists of two half-cycles with precursor and reactant gas exposures. The exposures are separated by pump and/or purge steps. Repeating this cycle leads to an ALD process.

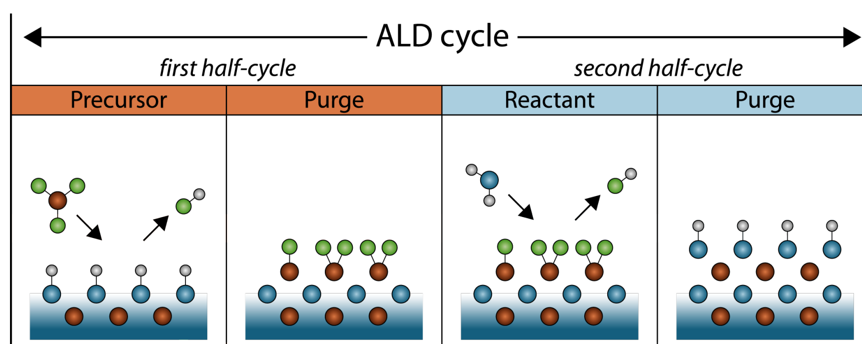


*Figure 1.1:* Basic configuration of one ALD cycle consisting of a precursor dose and a purge step in the first half-cycle, and a reactant dose and purge step in the second half-cycle.

In the first half-cycle, the precursor reacts with the starting substrate surface. This precursor is a vapor that consists of molecules containing the element of the material to be deposited. The precursor molecules only react with the initial surface groups and do not react with the new surface groups that are formed when the precursor molecules adsorb. Consequently, the surface reactions stop when all surface groups have reacted. This is the so-called self-limiting property of the reaction. The by-products that are formed and the excess precursor are subsequently removed by a purge and pump step.

In the second half-cycle, the surface is exposed to a reactant gas. This gas reacts with the surface groups that are formed during the first half-cycle and new surface groups are created. The surface reaction is also self-limiting and stops when all surface groups (of the first half cycle) have reacted. All the by-products are removed again with a purge and pump step. After these four steps, together one ALD cycle, a (sub)monolayer of

material has been deposited. Since the surface is covered again with surface groups that can react with the precursor, the cycle can be repeated until the desired thickness is reached, which leads to thickness control on nanometer scale.

The achievement of saturation of the self-limiting half-reactions is very important for an ALD process. By choosing sufficiently long dosing times under the right conditions (i.e. pressure and temperature) saturation is reached because all the surface groups reacted in every half-reaction. This means that there is a maximum of precursor and reactant gas that can react with the surface and this leads to a constant amount of material that is deposited every cycle. Furthermore, the two half-reactions are separated by purge (and pump) steps which ensure that the precursor and reactant gases are not present simultaneously. No gas-phase reactions between these gases can occur and therefore no chemical vapor deposition (CVD) growth takes place. The result of the above properties of ALD is that the deposited film is very smooth, continuous and pinhole-free.

## 1.2 Platinum ALD

Platinum (Pt) is a noble metal with many applications in microelectronics and catalysis [1]. Pt has a high chemical stability in oxidizing environments and excellent electrical properties. Aaltonen *et al.* [3] introduced the thermal Pt ALD process consisting of precursor $MeCpPtMe_3$ (methylcyclopentadienyl(trimethyl)platinum) and reactant $O_2$ (oxygen) gas exposure. The reaction mechanism of Pt ALD will be discussed in this paragraph. During the process, several surface reactions occur and this is schematically shown in Figure 1.2.

The starting surface is covered with oxygen atoms formed during the previous ALD cycle. In the first half-reaction, $MeCpPtMe_3$ molecules react with the oxygen atoms on the Pt surface and $CO_2$ and $H_2O$ are the reaction products of this combustion-reaction, which was reported by Aaltonen *et al.* [3]. As soon as oxygen at the surface becomes depleted, the precursor molecules continue to react in oxygen lean conditions. The precursor ligands undergo catalytic dehydrogenation resulting in adsorbed hydrocarbon species and $H_2$ as a reaction product, while incomplete combustion of the ligands can give some CO [4, 5]. Hydrogenation of Me species may be the explanation [1] for the observed formation of $CH_4$ during the $MeCpPtMe_3$ pulse which was was also detected as a reaction product by Kessels *et al.* [6]. As a result of the dehydrogenation reactions, the Pt surface becomes covered with a carbonaceous layer.

During the second half-reaction, this carbon-rich layer reacts with oxygen which gives $CO_2$ and $H_2O$ as reaction products. After complete removal of the carbonaceous species, some oxygen atoms are dissociated on the Pt surface and then the cycle starts again with precursor dosing.

Above mentioned ALD process consists of alternating precursor and reactant exposure half-reactions that are repeated cyclewise (ABAB). Plasma-assisted ALD involves the exposure of the surface to a plasma in step B, and allows for deposition at reduced substrate temperatures [7]. Pt ALD at low-temperatures is investigated by Mackus et al. [1], who developed process ABC and ABC* consisting of $MeCpPtMe_3$ precursor dos-

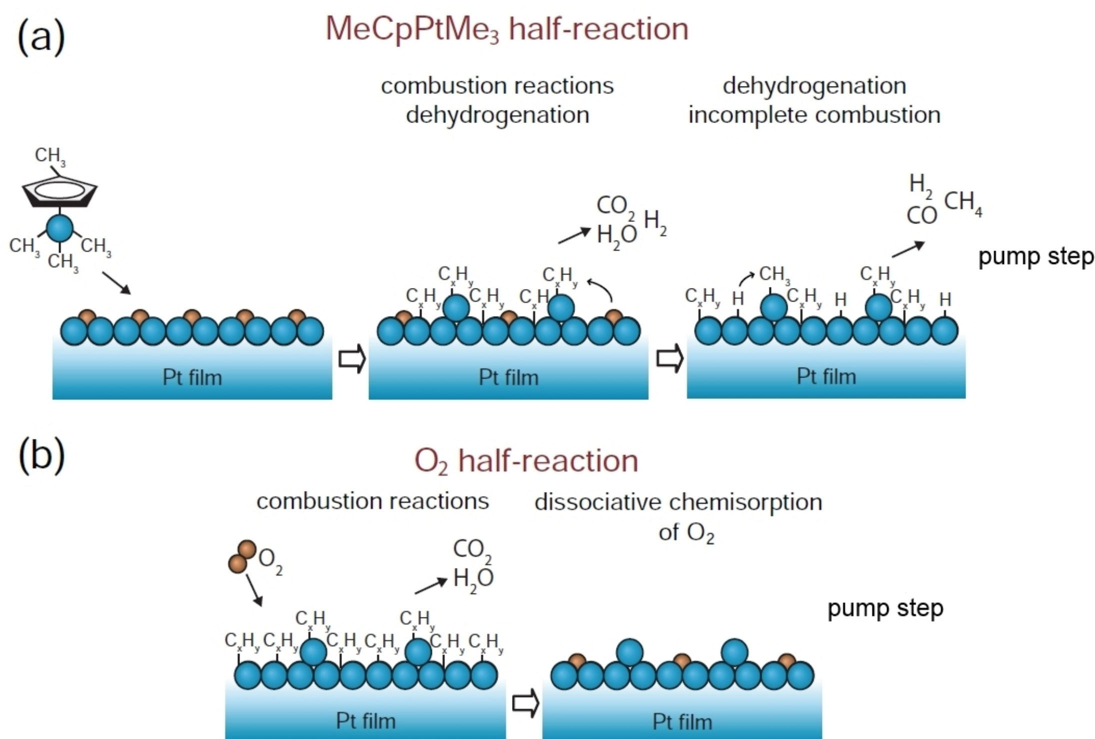


*Figure 1.2:* Schematic representation of the thermal Pt ALD process. *(a)* The starting surface is a Pt film covered with O atoms. Combustion reactions between oxygen species and precursor ligands, incomplete combustion and dehydrogenation result mainly to the formation of $CO_2$ and $H_2O$ and further to CO and $H_2$ and in addition also $CH_4$ is formed. *(b)* In the $O_2$ half-reaction, combustion of the remaining precursor ligands takes place and the surface is covered again with oxygen.

ing (A), $O_2$ plasma exposure (B) and $H_2$ gas exposure (C) or $H_2$ plasma exposure (C*). The reaction mechanism of process ABC, which is almost the same as process ABC*, was investigated by gas-phase Fourier transform infrared spectroscopy (FT-IR) [1]. FT-IR measurements have shown that, during the $O_2$ plasma exposure, $H_2O$ and $CO_2$ are created from combustion reactions. Furthermore, the FT-IR spectrum during process ABC shows the formation of $H_2O$ during the $H_2$ plasma step, implying that a significant amount of oxygen resides at the surface after the $O_2$ plasma pulse. It is known that an $O_2$ plasma is able to oxidize the near-surface region of a Pt film which results in thin layer $PtO_x$ at the surface. The exposure to $H_2$ plasma leads to the reduction of this $PtO_x$ film in Pt surface and releases $H_2O$ as reaction product.

## 1.3 Aim of this research

The main goal of this study is to optimize the Pt ALD process on the FlexAL setup. Previously, thermal Pt ALD as well plasma Pt ALD processes were optimized on the ALD-I setup and these results [1] are taken as starting point for this study. The ex-

periments consist primarily of measuring saturation curves with different conditions for the precursor and reactant dosing steps. The optimization is done for thermal ALD at 300°C and plasma ALD at room temperature (RT). The nucleation and growth of Pt deposition is studied with the use of two *in situ* techniques, which are: spectroscopic ellipsometry (SE) and optical emission spectroscopy (OES).

A second goal is to investigate the differences between the FlexAL and ALD-I setups. Results from Mackus on the ALD-I setup and results of this study are compared. An important element of the research is also to take the high cost of the $MeCpPtMe_3$ precursor into account and therefore to dose as efficiently as possible.

The initial goal for this study was to investigate Pt nanoparticle deposition with control of the particle size distribution. Therefore, the process introduced by Mackus [1], must be optimized and this optimization was taking as starting point for this study.

The report is organized as follows. In chapter 2, the experimental setup and the ALD processes for thermal ALD and plasma ALD are discussed. This is followed by the description of the used diagnostics. In chapter 3, results for the optimization of the thermal Pt ALD process (at 300°C) as well for the plasma Pt ALD process (at room temperature) are presented. For the optimization of the thermal ALD process, saturation curves of the two half-cycles and nucleation curves are measured by SE. For the optimization of the plasma Pt ALD process, saturation curves and emission spectra were measured by SE and OES, respectively. In chapter 4, the results from SE and OES measurements during the different steps of the plasma ALD process are compared and the optimized plasma ALD process is discussed. Subsequently, the differences and similarities between the FlexAL and ALD-I setup are discussed. At the end, a conclusion is drawn and an outlook is given.

# 2 Experimental Setup

## 2.1 FlexAL setup

The FlexAL setup is used in this research for the deposition of Pt by ALD. The setup offers capabilities for remote plasma ALD and thermal ALD in one single ALD reactor. Figure 2.1 shows a schematic representation of the FlexAL reactor. The setup consists

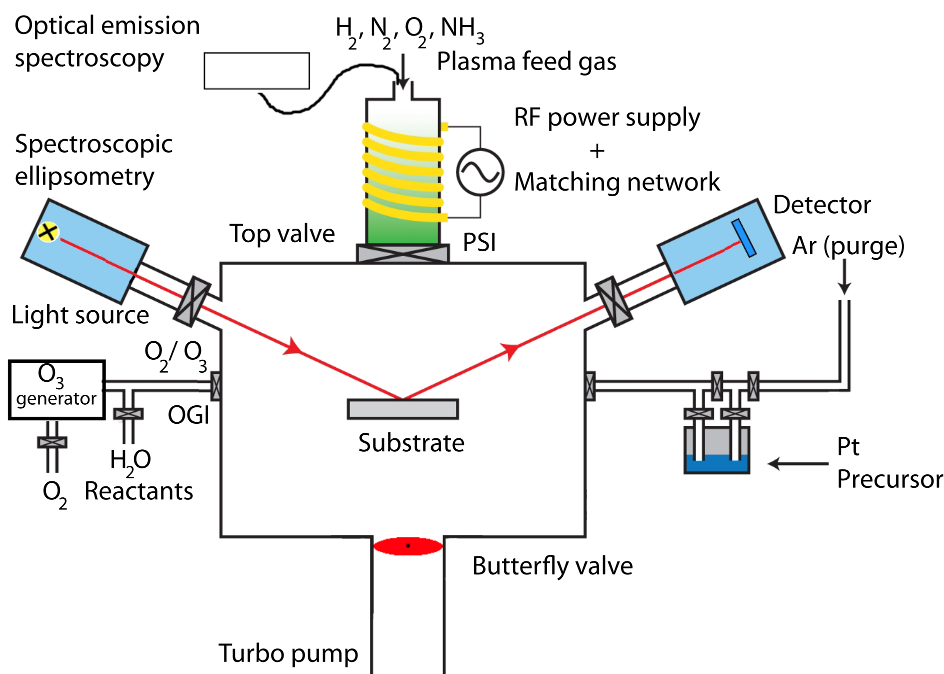


*Figure 2.1:* Schematic representation of the FlexAL setup for thermal and plasma ALD. The figure shows the main deposition chamber with several inlets for reactant gases and precursor dosing, and the *in situ* spectroscopic ellippsometer. The plasma source inlet (PSI) and ozone generator inlet (OGI) are used for oxygen dosing. The load lock is not shown.

of a load lock and a reactor chamber, which can be separately pumped to pressures in the range of $10^{-5}$ and $10^{-6}$ mbar, respectively. The deposition takes place in the reactor chamber which is connected to a pump unit, a plasma source, and several precursor and gas inlets. The sample is placed on the substrate holder in the load lock and after evacuating this load lock to vacuum, the substrate table is moved to the deposition chamber. The heated area which carries the substrate holder, called the substrate heater, and the reactor wall of the FlexAL reactor are heated to certain temperatures, depending on the process. In this work, the substrate heater is heated to a set temperature of 300°C and the reactor wall to 120°C for thermal ALD, while both elements are kept at room temperature by switching off the heating for plasma ALD. It is important to take into account that the temperature of the sample is not equal to the set temperature. The sample temperature is 25°C to 100°C lower for set temperatures in the range of 100°C to 500°C. The difference between the set temperature and the sample temperature

increases for increasing setpoint temperatures, which is investigated by Braeken [8]. The whole reactor is computer-controlled which makes it possible to perform fully-automated depositions.

The plasma is generated by a remotely-placed inductively-coupled plasma source. The input power is 100 W and is controlled by an automated matching network. Input values for the capacitors of the the matching network were chosen such that the power quickly reaches the input power of 100 W. The input values for capacitor one and two are 48.1% and 52.0% for the oxygen plasma and 57.9% and 49.4% for the hydrogen plasma respectively. A wide range of gases such as Ar, $H_2$, $N_2$ and $O_2$ are connected via gas inlets to the plasma source. The flow of the gases are controlled by mass flow controllers.

The pump unit of the chamber consists of a turbo-molecular pump and a rotary vane pump which evacuate the chamber to pressures in the $10^{-6}$ mbar range. The operating pressure in the chamber during processing can be set using an automated pressure controller (APC), which comprises a fast (90 ms open-close) butterfly valve located in between the turbo pump and the chamber. A butterfly valve is a valve with a round disc that rotates on its axis. When the valve is closed (0 degrees), the disc in the valve is positioned such that it completely blocks off the flow direction. When the valve is fully open (90 degrees), the disc is rotated a quarter turn such that it allows an almost unrestricted flow of the gases. Pressure can be controlled by setting the disc at a fixed angle, which can be chosen between 0 degrees and 90 degrees. A small angle ensures that the gases remain longer in the chamber, which leads to higher pressures. The pressure can also be controlled by choosing a fixed pressure in which the angle of the disc is automatically changes to a certain angle.

Since $MeCpPtMe_3$ is a powder at room temperature, the precursor is heated to obtain the required vapor pressure for dosing the precursor in the chamber. Precursor temperatures around 30° are chosen as set point but after some experiments it has been found that the precursor dosing times became too long to achieve saturated growth. Heating the precursor to 40° leads to shorter dosing times to achieve saturation. However, a higher precursor temperature gives a higher precursor vapor pressure which leads to more precursor dosing. Argon is used as carrier gas for delivery of the precursor vapor to the reactor chamber.

The chamber has various gas inlets for oxygen gas. The ozone generator inlet (OGI) can be used as oxygen gas inlet. By turning off the ozone generator, oxygen gas flows from the outlet of this generator to the gas inlet of the chamber. Also the $O_2$ line connected to the plasma source can be used for oxygen dosing (gas as well as plasma). For oxygen dosing via the plasma source inlet (PSI), the top valve at the top of the chamber must be opened. The PSI is larger in comparison with the OGI and it takes therefore longer to open the top valve. Furthermore, by opening the top valve, the chamber volume increases more because the volume of the plasma source must be added. A second difference between oxygen dosing via the PSI or OGI is the evolution of the oxygen pressure. Figure 2.2 shows the oxygen pressure as function of time. It is important to take the pressure evolution into account. From Figure 2.2 it becomes clear that during

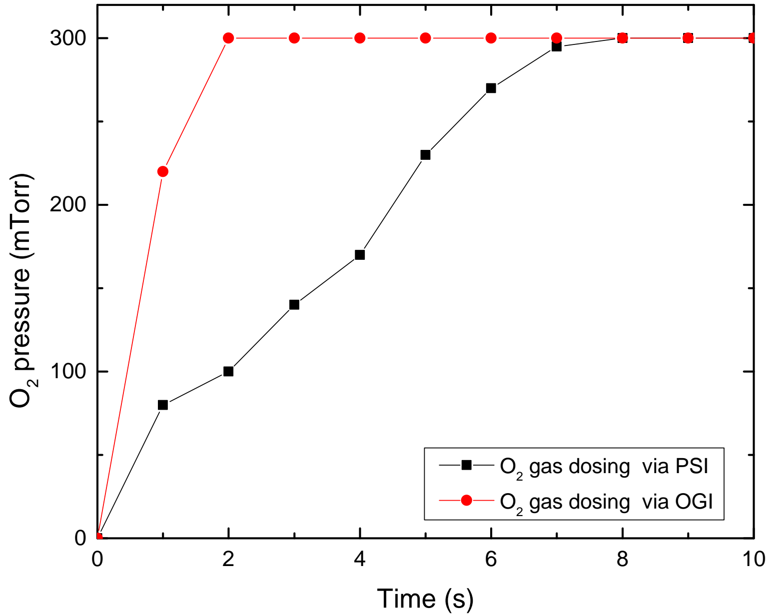


*Figure 2.2:* $O_2$ pressure as a function of time for gas dosing via the plasma source inlet (PSI) or via the ozone generator inlet (OGI). The $O_2$ pressue was set to 300 mTorr for 10 s.

the oxygen dosing, the pressure is not directly equal to the set pressure of 300 mTorr. However, the pressure of the oxygen dosage via the OGI reaches the set pressure faster. Dosing via the OGI and PSI are both explored in the experiments.

In a study of Mackus [1] was shown that for the deposition of supported Pt particles for catalysis applications, an intermediate oxygen pressure of 300 mTorr should be selected, since there is no growth for low oxygen pressure and a large spread in the particle size distribution for high oxygen pressures. Because of the interesting catalysis application, 300 mTorr oxygen pressure was taken as starting point for this study.

Furthermore, a spectroscopic ellipsometry (SE) system is mounted to enable *in situ* thickness measurements. The SE is hooked up to the reactor and consists of a light source and a detector, which are placed at a fixed angle. This angle is close to the Brewster angle of Silicon (68 °) to maximize the signal intensity of the reflection [9]. All *in situ* SE measurements were done using a J.A. Woollam, Inc M2000FI visible and near-infrared ellipsometer, over the photon energy range from 0.75 eV to 5.5 eV and a J.A. Woollam, Inc M2000U visible ellipsometer, over the photon energy range from 1.2 eV to 5.5 eV. A port positioned on top of the plasma source was used for optical emission spectroscopy (OES). The light emission from the plasma is collected by a quartz optical fiber which is coupled to an Ocean Optics USB4000 spectrometer. This spectrometer has a wavelength detection range of 200-1100 nm and a resolution of approximately 1 nm. The SE and OES settings will be discussed in paragraph 2.3 and 2.4, respectively.

## 2.2 Platinum ALD

Pt ALD is achieved in this project via two processes: thermal ALD at 300°C and plasma ALD at room temperature. These ALD processes consist of a few steps which are illustrated in Figure 2.3.

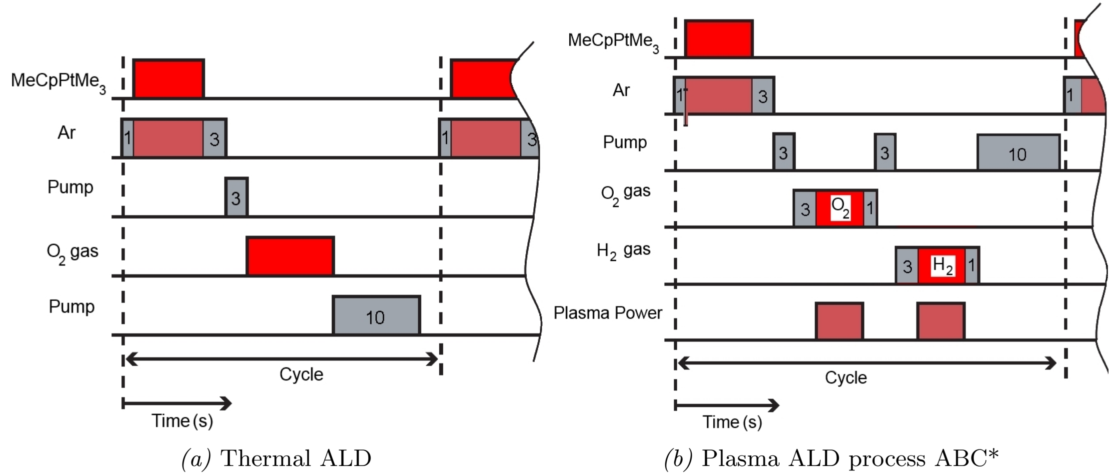


*(a)* Thermal ALD *(b)* Plasma ALD process ABC*

*Figure 2.3:* A schematic view of: a typical *(a)* thermal ALD cycle; *(b)* plasma ALD cycle for deposition at room temperature. The duration of the $MeCpPtMe_3$, $O_2$ gas/plasma and $H_2$ plasma exposure were varied. The process in *(b)* consists of the same precursor step as in *(a)*. By varying the $MeCpPtMe_3$ dose time, also the duration of the precursor carrier gas (Ar) changes. The plasma power is switched on during the $O_2$ and $H_2$ plasma exposure steps.

The thermal ALD cycle (Figure 2.3a) contains two half cycles. The precursor container is heated to 40° and the substrate heater to 300°C. In the first half-cycle, precursor dosing takes place and Ar (50 sccm) is used as carrier gas. The precursor dosing time can be varied. Before precursor dosing, 1 s Ar flow (50 sccm) is added to stabilize the Ar gas flow. The precursor dosing is concluded with 3 s Ar purge (100 sccm) to remove excess precursor and reaction products from the process chamber in order to prevent CVD on the substrate. After the Ar purge, the reactor is pumped down for 3 s.

The second half-cycle begins with 300 mTorr oxygen dosing and ends with ten seconds pump down. The oxygen dosing time was varied. Typically, the precursor dosing time is chosen in saturation, to investigate the oxygen dosing time and vice versa. The pressure of Ar and precursor before and during the precursor dosing are controlled by setting different valve positions (10°, 35° and 45°) and different pressures, which results in pressures in the range of 5 mTorr up to 170 mTorr. Furthermore, measurements with high and low oxygen pressure were done. For the plasma ALD process at room temperature, Mackus developed a process consisting of $MeCpPtMe_3$ precursor dosing (A), $O_2$ plasma exposure (B) and $H_2$ plasma exposure (C*). The recipe, called process ABC* [1], is illustrated in Figure 2.3b. The precursor container is also heated to 40°C and the table heater and wall heater are turned off which results in a temperature of

25°C. Process ABC* contains the same precursor step as the thermal ALD process. Pump times are chosen 3 s after step A, 6 s after step B and 10 s after step C. The pump step after step C was chosen as long as 10 s, since it takes relatively long to evacuate the $H_2$ molecules and the $H_2O$ molecules formed in the surface reactions during the $H_2$ pulse [1]. Each plasma step (both $O_2$ and $H_2$) is preceded by 3 s gas dosing (to obtain a stabilized gas flow) and concluded with 1 s gas dosing after switching off the plasma. The gases $O_2$ and $H_2$ were set to a pressure of 12 mTorr by setting the butterfly valve at 30°. The pressure of the Ar and precursor gas, before and during precursor dosing, was controlled by setting the butterfly valve at 35° which results in a pressure of 11-12 mTorr. To optimize the ABC* recipe, saturation curves for step A, B and C* were measured by SE.

## 2.3 Spectroscopic Ellipsometry

The optical technique spectroscopic ellipsometry (SE) is used for determining the film thickness of a deposited film [10]. SE measures the change in polarization of light, after it is reflected from the film into the detector. An ellipsometer system consists of a light source and a detector unit as shown in Figure 2.4.

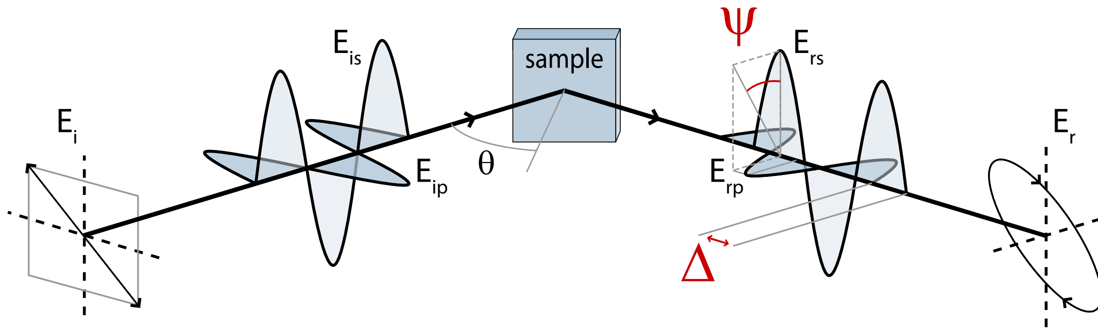


*Figure 2.4:* Schematic overview of a SE measurement. An incoming light beam with a certain polarization is traveling towards the sample. When the light beam is reflected on the sample, the polarization has changed. This change in polarization is measured by measuring $\Psi$ and $\Delta$, the spectroscopic parameters as a function of the wavelength. $\theta$ is the angle of incidence.

In a SE measurement, the polarization of the light-beam is known and the detector measures the ratio of the p- and s-polarization reflection amplitudes, via two parameters $\Psi$ and $\Delta$. The ratio between the electric field before ($E_{ix}$) and after reflection($E_{rx}$) gives the Fresnel coefficient $R_x$ (with $x$ = s or p). These parameters are related to the complex Fresnel reflection coefficients via the complex ellipsometric parameter $\rho$:

$$\rho = \frac{R_p}{R_s} = \frac{E_{rp}/E_{ip}}{E_{rs}/E_{is}} = \tan\Psi \exp(i\Delta) \tag{2.1}$$

where $R_p$ and $R_s$ are the complex Fresnel reflection coefficient for p- and s-polarized light, respectively. The change in polarization is determined as a function of the wave-

length and from these data, the film thickness and the optical constants can be deduced. The optical constants are expressed in the refractive index $n$ and extinction coefficient $k$. More common are the real ($\varepsilon_1$) and imaginary ($\varepsilon_2$) parts of the complex dielectric function $\varepsilon$ with the definitions $\varepsilon_1 = n^2$-$k^2$ and $\varepsilon_2 = 2nk$. $\varepsilon_1$ and $\varepsilon_2$ are Kramers-Kronig consistent. The spectroscopic parameters are collected as a function of wavelength, for the angle of incidence $\theta$. Furthermore, the SE data has to be interpreted using an appropriate optical model for the Pt film and its substrate ($SiO_2$ or $Al_2O_3$) on c-Si. The thickness and the dielectric function of the individual layers should be taken into account in this model. The model of the investigated layer is fitted to the measured data as closely as possible (while the models of the other layers are fixed), and the corresponding thickness and dielectric function is calculated. The accuracy of the model can be evaluated with the mean square error (MSE). The MSE can be determined from the difference of $\Psi$ and $\Delta$ as derived from the model and the experimental values. The B-spline model is used for the deposited Pt film and is discussed in detail by Thissen [9].

The SE measurements were done after every 10 cycles by opening the gate valves to the SE light source and detector for 40 seconds. The SE software then starts automatically a high-accuracy measurement of 30 seconds. Growth rate values were determined from the slopes of the graphs in which the thickness is plotted as a function of the number of ALD cycles. Saturation curves were measured on substrates with a minimal Pt layer of 10 nm to exclude nucleation effects in the analysis. For measuring saturation curves, all steps must be chosen in saturation except the step for which saturation is measured. Therefore, the duration of one step is varied, while taking the duration of the other steps sufficiently long to ensure saturation of surface reactions. Optimization is done by determine saturation curves of all steps by SE measurements. In addition, nucleation curves were measured on Si substrates covered with $\sim$ 250 nm $Al_2O_3$.

## 2.4 Optical Emission Spectroscopy

Optical Emission Spectroscopy (OES) is an easy-to-implement and valuable tool to study thin film growth by plasma-assisted ALD [11]. In plasma-assisted ALD, one of the main steps is the plasma exposure of the surface. OES uses the fact that a plasma emits light. Excited states of the atoms and molecules which are present in the reactor are in most cases created through collisions between plasma species with electrons. From the decay of these excited atoms, an emission spectrum with emission lines originate. The existence of particular emission lines indicates the presence of particular species in the plasma. With the OES method, reactant species delivered to the surface by the plasma can be identified. Furthermore, OES gives insight into the surface reaction products and, as a consequence, on the reaction mechanism of the deposition process. Time-resolved measurements bring out information about the amount of precursor dosing and length of plasma exposure needed to saturate the self-limiting half reactions. This is useful for the optimization of the ALD process. The time-resolved measurements show mainly the intensity of an emission line, characterized by a wavelength. Meanwhile, in an ionizing plasma, electron excitation is predominant. Therefore the decay of species from level $q$ to level $p$ by spontaneous emission is distinctive. The wavelength of an emission line $\lambda$ is

determined by the photon energy corresponding to the transition of level $p$ with energy $E_p$ to level $k$ with energy $E_k$,

$$\lambda = \frac{h \cdot c}{E_p - E_k} \tag{2.2}$$

with $h$ and $c$ Planck's constant and the speed of light, respectively. The emission intensity is proportional to the density of electronically excited species and is defined by the product of the Einstein coefficient $A_k$ of a spontaneous emission process and the population density of the excited level $n_p$:

$$I_{pk} = n_p \cdot A_{pk}. \tag{2.3}$$

OES measurements are recorded during the $O_2$ plasma and $H_2$ plasma step. Peaks in the spectra are related to presence of particular species. From time-resolved measurement, emission at certain wavelengths are followed in time and this gives insight into the reactions that takes place.

# 3 Results

The main goal of this project is to optimize Pt ALD on the FlexAL setup for thermal ALD and for plasma ALD at room temperature. The optimization for the thermal ALD process by SE is discussed in section 3.1.1 which is concluded with nucleation curves (presented in section 3.1.2) to investigate the growth behavior of thermal Pt ALD. The plasma ALD process at room temperature is optimized with SE and OES measurements which are included in section 3.2.1 and section 3.2.2, respectively.

## 3.1 Thermal Pt ALD

### 3.1.1 Saturation of half-reactions

To optimize the thermal Pt ALD process, all the surface reactions must be in saturation. Therefore, the growth rate is measured as function of the number of cycles for the precursor and reactant half-reactions. To measure the saturation curve of the precursor half-reactions, the reactant dosing is taken sufficiently long to ensure saturation of the reactant half-reaction. Figure 3.1 shows the saturation curve of the precursor half-reaction in which the oxygen dosing time was chosen 10 s, such that the oxygen half-reaction is in saturation. The precursor dosing time was varied from 3 s until 15 s and the precursor pressure is about 9.5 mTorr. From the graph becomes clear that after 8 s,

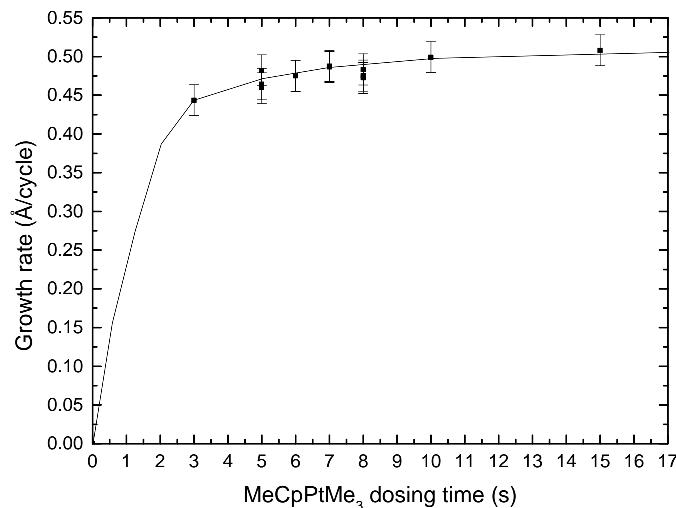


*Figure 3.1:* Saturation curve showing the growth rate as a function of the $MeCpPtMe_3$ dosing time, as measured by *in situ* spectroscopic ellipsometry. It concerns a thermal ALD process with 10 s 300 mTorr (50 sccm) $O_2$ dosing (via the plasma source inlet). The final pressure of the Ar and precursor gas during the precursor dosing is about 9.5 mTorr, whereas the butterfly valve was put under an angle of 35°. The black line serves as a guide to the eye.

saturated ALD growth takes place. The graph reveals that a $MeCpPtMe_3$ dosing time of 8-10 s is required to obtain self-limiting precursor adsorption. This required precursor dosing time is long in comparison with dosing times on the ALD-I setup. Comparison with the ALD-I setup is discussed more in detail in section 4.2.

To optimize the oxygen dosing time, the precursor dosing was chosen in saturation, which is from above-mentioned results 8 s. The results of the *in situ* SE measurements are shown in Figure 3.2. Measurements were done with oxygen dosing via the PSI and

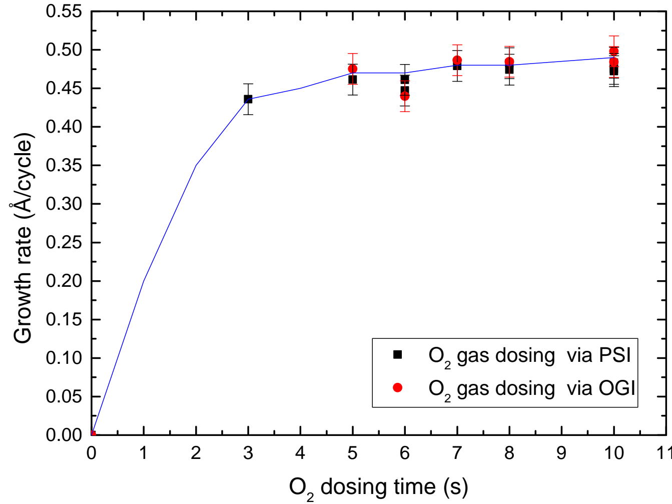


*Figure 3.2:* Saturation curve showing the growth rate as a function of the $O_2$ dosing time, as measured by *in situ* spectroscopic ellipsometry. Measurements are done by oxygen dosing via the plasma source inlet (PSI) and ozone generator inlet (OGI). It concerns a thermal ALD process with 8 s 9.5 mTorr precursor dose (with 50 sccm Ar) and 300 mTorr $O_2$ dose (50 sccm). The final pressure of the Ar and precursor gas during the precursor dosing is about 9.5 mTorr, whereas the butterfly valve was put under an angle of 35°. Oxygen was dosed via the PSI. The blue line serves as guides to the eye.

OGI with an oxygen pressure of 300 mTorr. The oxygen dosing time is varied from 3 s until 10 s. The graphs shows that the half-reactions were in saturation after 5 s and it becomes clear that dosing via the PSI or OGI gives approximately the same growth rate within the uncertainty of the measurement. 5 s oxygen dosing is required for saturated ALD growth.

The results presented above lead to an optimized thermal ALD process (see Table 3.1) with a growth rate of ~0.49 ± 0.02 Å/cycle which is in accordance with results on the ALD-I ~0.50 ± 0.01 Å/cycle [1].

### 3.1.2 Nucleation behavior

Next, the nucleation behavior of the process was investigated. To this end, the thickness of the deposited film was measured, with *in situ* SE, as a function of the number of cycles (see Figure 3.3). Oxygen was dosed via the PSI and the OGI.

Characteristic for all nucleation curves is that a growth delay occurs in the first cycles,

*Table 3.1:* Recipe of a thermal ALD process optimized with $MeCpPtMe_3$ and $O_2$ pulse time chosen in saturation. The final pressure of the Ar and precursor gas during the precursor dosing is about 9.5 mTorr, whereas the butterfly valve was put under an angle of 35°. During the Ar purge, the butterfly valve was fully open (90°).

| Precursor step | Pump down | Reactant step | Pump down |
|---|---|---|---|
| 1 s Ar 50 sccm<br>8 s $MeCpPtMe_3$ dosing with Ar 50 sccm<br>3 s Ar purge 100 sccm | 3 s | 5 s 300 mTorr $O_2$ 50 sccm | 10 s |

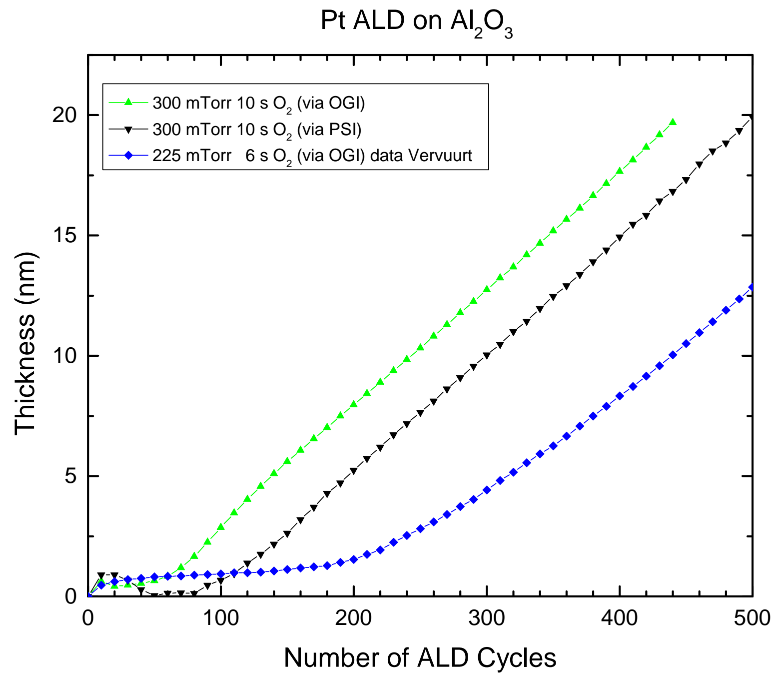


*Figure 3.3:* Nucleation curves showing the thickness as a function of the number of ALD cycles measured by *in situ* spectroscopic ellipsometry. Measurements are done for several $O_2$ pressures and dosing times and were performed on $Al_2O_3$ substrates. Oxygen is dosed via the inlets of the ozone generator (OGI) or the plasma source inlet (PSI). The two 300 mTorr measurements concern a thermal ALD process described by Table 3.1. Data from experiments of Vervuurt, which includes 3 s $MeCpPtMe_3$ dosing with 6 s 225 mTorr oxygen dosing on the FlexAL setup, were also added.

ranging from 40 cycles to 220 cycles. Remarkable is the difference in nucleation behavior of the two 10 s $O_2$ dosing depositions. The growth delay[1] is deduced from the nucleation curves and is 40 and 95 cycles for dosing via the OGI and PSI, respectively. The difference is caused by the oxygen exposure (i.e. pressure x time), which is obtained from the

[1] The growth delay is deduced from the nucleation curves by extrapolating the linear part of the graph to the y-axis and read out the x-intercept (number of ALD cycle).

integration of the curves of Figure 2.2. The exposure for dosing via the OGI is 1.35 times larger than for dosing via the PSI. Furthermore, the experiment of Vervuurt [12] with 225 mTorr oxygen dosing shows a clear difference in nucleation behavior. It has a larger growth delay (220 cycles) which is probably caused by the fact that 3 s precursor dosing was too short. The first half-reaction is therefore not in saturation which leads to a larger growth delay. It can be concluded that it is essential to choose both half-reactions in saturation. In the experiment with 10 s oxygen dosing via the PSI, a local maximum occurs in the nucleation curve. This is probably caused by the SE software in which the dielectric function could not be fitted well in the first cycles.

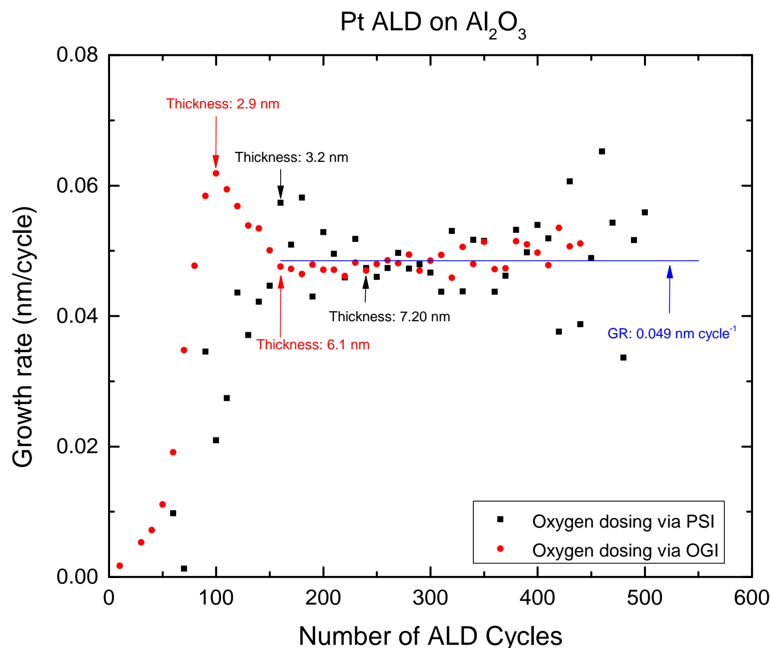


*Figure 3.4:* The growth rate as function of the number of ALD cycles for dosing via the plasma source inlet (PSI) and ozone generator inlet (OGI). It concerns a thermal ALD process with 8 s 9.5 mTorr precursor dose (with 50 sccm Ar) and 300 mTorr $O_2$ dose (50 sccm). The final pressure of the Ar and precursor gas during the precursor dosing is about 9.5 mTorr, whereas the butterfly valve was put under an angle of 35°. Several thickness are mentioned. The blue line serves as guide to the eye.

After a growth delay, the growth rate becomes constant and equal for both optimized processes (with 10 s 300 mTorr $O_2$). This is confirmed by determining the growth rate as a function of the number of ALD cycles form the nucleation curves (see Figure 3.4). The growth rate is calculated by taking the difference in thickness of two consecutive nucleation data points (separated by 10 cycles) and deviding this number by ten, such that the unit is nm/cycle. An average growth rate of 0.049 nm for both processes was found, calculated from the part of the graph when the growth rate is constant. The growth rate is constant after 160 and 240 cycles for dosing via OGI and PSI respectively. From the graph becomes also clear that, before the growth rate is constant, the growth rate is momentarily higher. A peak, which indicates a higher growth rate, occurs around

a thickness of 2.9 nm (via OGI) and 3.2 nm (via PSI). Around 6-7 nm, the growth rates become constant. This is typical nucleation behavior for type 2 substrate-inhibited ALD growth [13]. The behavior was also found from Pt ALD experiments of Thissen [9]. The peaks and the constant growth rates are probably caused by island growth which is typical for Pt growth on $Al_2O_3$ substrates [1]. Initially islands are formed and grow in size. After a while, the island partly overlap each other which is called island coalescence. Finally, the islands are fully merged. The island shape may explain why the growth rate is momentarily higher. The deposition area of islands is namely larger than a continuous, straight film and this probably leads to higher growth rates. However, further research in island growth, for example by simulating different island shapes and their nucleation behavior, could confirm this.

## 3.2 Pt plasma ALD at room temperature

For depositing Pt films at room temperature, process ABC* is used. From previous results, the duration of precursor dosing is chosen 8 s for measuring saturation curves for the $O_2$ and $H_2$ plasma step. Furthermore, the $O_2$ plasma exposure time is varied with constant $H_2$ plasma exposure time and vice versa. The results are presented in section 3.2.1. In section 3.2.2, spectra at the begin and end of the $O_2$ plasma and $H_2$ plasma step are shown. The intensity of some emission lines are followed in time by time-resolved measurements.

### 3.2.1 Process optimization by SE

Process ABC* consists of three steps in which two of the steps are taken in saturation for measuring the saturation of the other step. During the measurement of the saturation curve of step B, the dosing and esposures times in step A and C are taken sufficiently long to ensure saturation of these steps. Saturation curves were measured for the $O_2$ and $H_2$ plasma reactant which can be seen in Figure 3.5. From Figure 3.5a it becomes clear that both curves saturate to a growth rate of $\sim 0.42 \pm 0.02$ Å/cycle and that $O_2$ saturation is reached with 5 s exposure. The difference in saturated growth rate for 5 s and 10 s $H_2$ plasma exposure (with 5 s or more $O_2$ plasma exposure) is within the uncertainty of the measurement. After the $O_2$ plasma pulse, a thin layer of $PtO_x$ is present at the Pt surface. The $H_2$ plasma reduces this thin layer and from Figure 3.5b it becomes clear that 0.5 s $H_2$ plasma exposure is long enough to achieve this. Reduction therefore goes relatively quickly. The curve saturates to the same growth rate of $\sim 0.42 \pm 0.02$ Å/cycle.

From the above-mentioned results, it is concluded that step B and C are in saturation for plasma exposures of 5 s and 0.5 s respectively. To investigate the saturation of the precursor (step A), sufficiently large plasma exposure times of steps B (5 s) en C (5 s) were chosen. The results of the SE measurements with varying the precursor dosing time are shown in Figure 3.6. The curve shows also saturated ALD growth with a growth rate of $\sim 0.42 \pm 0.02$ Å/cycle and it becomes clear that 8 s dosing is sufficient to achieve

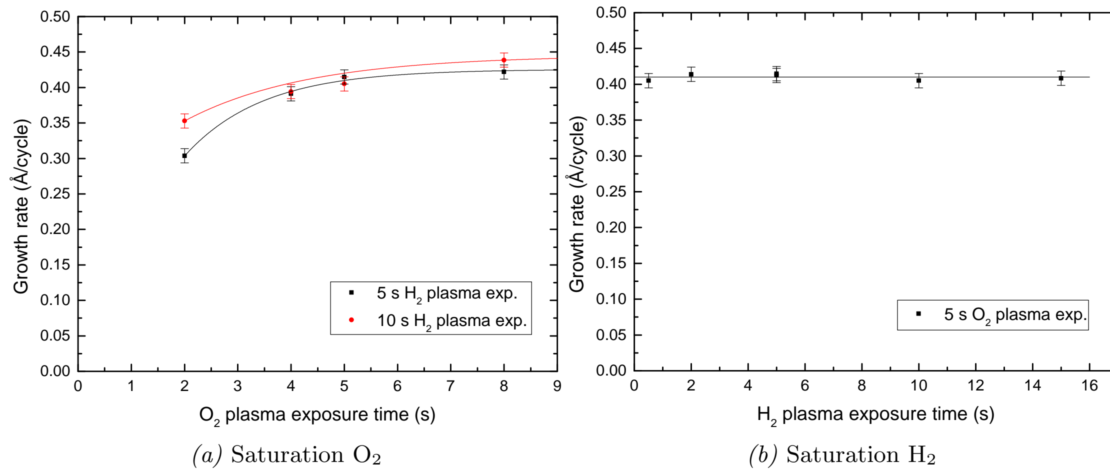


*(a)* Saturation $O_2$ *(b)* Saturation $H_2$

*Figure 3.5:* Saturation curves for the: *(a)* $O_2$ plasma step and *(b)* $H_2$ plasma step. The curves show the growth rate as a function of the $O_2$ or $H_2$ plasma exposure time, as measured by *in situ* spectroscopic ellipsometry. It concerns the ABC* recipe with 8 s $MeCpPtMe_3$ dosing. The lines serve as guides to the eye.

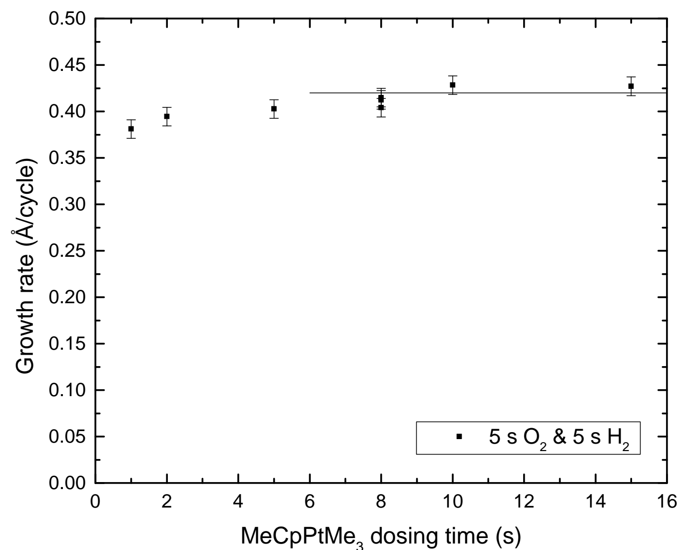


*Figure 3.6:* Saturation curve of $MeCpPtMe_3$ precursor step. The curve shows the growth rate as a function of the $MeCpPtMe_3$ dosing time, as measured by *in situ* spectroscopic ellipsometry. It concerns the ABC* recipe with 5 s $O_2$ plasma exposure and 5 s $H_2$ plasma exposure. The line serves as guide to the eye.

saturation. The growth rate is in agreement with results reported on the ALD-I setup ($\sim 0.40 \pm 0.04$ Å/cycle) [1].

### 3.2.2 Process optimization by OES

Process ABC* includes $O_2$ plasma exposure in step B and $H_2$ plasma exposure in step C. OES measurements were performed during these plasma exposures. Figure 3.7a shows spectra recorded during the first and last 30 ms of the $O_2$ plasma exposure. The emission

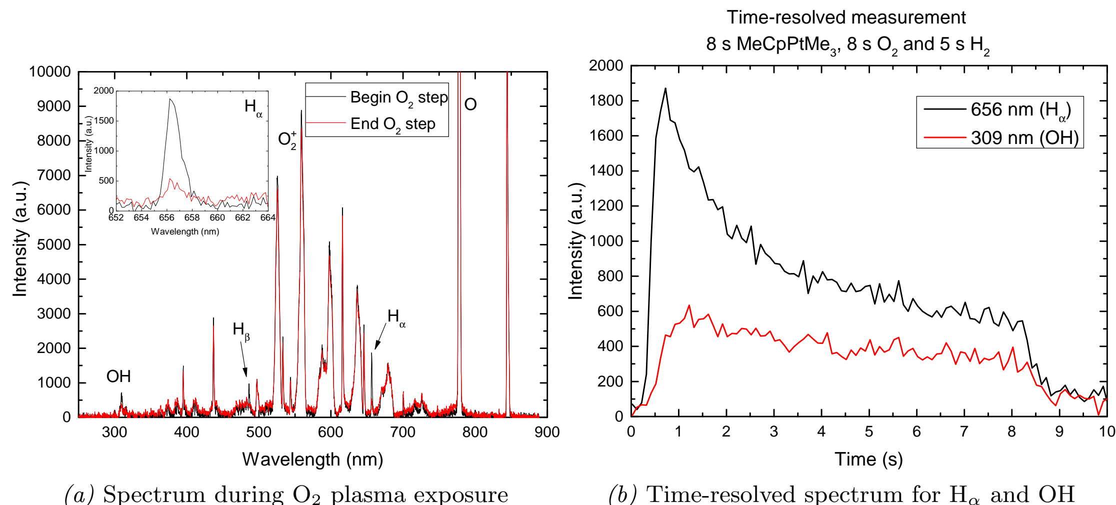


*(a)* Spectrum during $O_2$ plasma exposure *(b)* Time-resolved spectrum for $H_\alpha$ and OH

*Figure 3.7: (a)* Emission spectrum of an $O_2$ plasma exposure during a plasma ALD cycle. The spectrum was recorded after an $MeCpPtMe_3$ dosing step during the first and last 30 ms of the plasma exposure. In the inset a zoom of the spectra around the emission lines of $H_\alpha$ (656 nm). *(b)* Time-resolved measurements of emission lines at 656 nm and 309 nm, related to reaction products $H_\alpha$ and OH (A $^2\Sigma^+ \rightarrow$ X $^2\Pi$). The plasma was ignited at time t= 0.2 s for 8 s plasma exposure.

lines in these spectra are an indication of the presence of particular species. Therefore, OES gives insight into the plasma species and surface reaction products. The additional peaks present at start of the $O_2$ plasma pulse are related to the excited $H_\alpha$ (656 nm) and OH (A $^2\Sigma^+ \rightarrow$ X $^2\Pi$, 309 nm) species. The intensities of these peaks are decreased during the end of $O_2$ plasma pulse. $H_2O$ is one of the combustion reaction products during the oxygen step. Under influence of the $O_2$ plasma, dissociation of $H_2O$ takes place which leads to the excited $H_\alpha$ and OH species which are also measured in Figure 3.7. Emission lines of the dissociation reaction product $H_\alpha$ (656nm) are shown in more detail in the inset of Figure 3.7a. The presence of $H_\alpha$ and OH are an indication of the combustion reactions (with $H_2O$ as reaction product). Most of the other peaks in Figure 3.7a are related to $O_2$ plasma species. The intensity of emission at 777 nm (representative of O radical) is over-saturated which means that the intensity is too high for the spectrometer. It is remarkable that no CO and $CO_2$ emission was observed in the spectra while these species supposed to be formed in combustion reactions and were observed in other studies on the ALD-I [1].

In Figure 3.7b time-resolved measurements are shown for intensity at 656 nm ($H_\alpha$) and 309 nm (OH). The evolution of the intensity at 656 nm ($H_\alpha$) is probably a good indication for the presence of $H_2O$ in the plasma. The signal at 309 nm (OH) contains too

much background intensity in order to carefully analyze its evolution. The intensity at 656 nm ($H_\alpha$) decreases as function of the time and from Figure 3.7b it can be concluded that the intensity becomes constant to the background intensity, after 5 s $O_2$ plasma exposure. This means that after 5 s, $H_2O$ no longer is present which probably indicates the completion of the combustion reactions. According to above-mentioned, 5 s $O_2$ plasma exposure must be chosen for the optimization of the oxygen step.

OES data taken during the $H_2$ plasma exposure were also analyzed and the spectra are presented in Figure 3.8. From the comparison between the two spectra, most of the

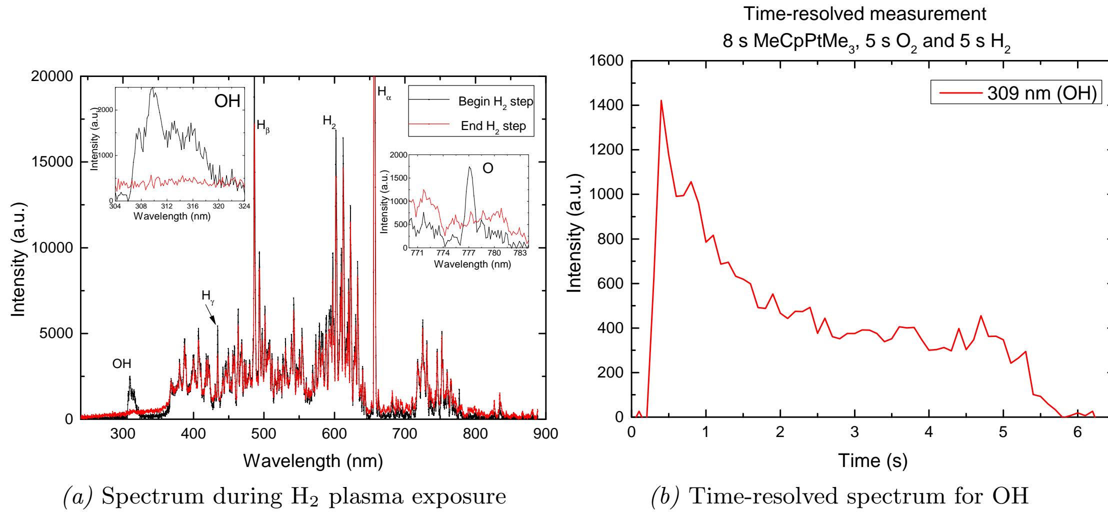


*(a)* Spectrum during $H_2$ plasma exposure *(b)* Time-resolved spectrum for OH

*Figure 3.8: (a)* Emission spectrum of an $H_2$ plasma exposure during a plasma ALD cycle which was recorded during the first and last 30 ms of the plasma exposure. In the insets, magnifications of the spectra around the emission lines of O (777 nm) and OH (308.9 nm). *(b)* Time-resolved intensities of emission lines at 777nm and 309 nm, related to reaction products O and OH. The plasma was ignited at time t= 0.2 s for 5 s plasma exposure.

peaks, related to hydrogen emission ($H_2$, $H_\alpha$, $H_\beta$ and $H_\gamma$), remain constant. However, two additional peaks present at the start of the $H_2$ plasma pulses are detected. These peaks are related to excited OH (A $^2\Sigma^+ \rightarrow$ X $^2\Pi$, 309 nm) and O (777.19 nm) species and magnifications around the emission lines are presented in the insets in the figure. The surface reaction that occur, during $H_2$ plasma exposure, is the reduction of the $PtO_x$ film to Pt. After the $O_2$ plasma pulse, a significant amount of oxygen resides at the surface. The $O_2$ plasma is able to oxidize the near surface region of the Pt film. Under influence of the $H_2$ plasma, the $PtO_x$ surface is reduced to Pt, in which $H_2O$ is the main reaction product [1]. Subsequently, $H_2O$ is dissociated in the plasma leading to excited $H_\alpha$ and OH species. Mainly OH is an good indication for the formation of $H_2O$ because the intensity of $H_\alpha$ is over saturated.

The time-resolved measurement for the intensity at 309 nm (OH) is shown in Figure 3.8b. After about 2.5 s plasma exposure, the intensity at 309 nm (OH) was constant to the background intensity which means that the reduction reaction (and the formation

of $H_2O$) is completed. Therefore, 2.5 s $H_2$ plasma exposure must be chosen to optimize the hydrogen step, according to OES measurements.

# 4 Discussion

## 4.1 Comparison SE and OES results

From studying the saturation (section 3.2.1) and (time-resolved) OES measurements, plasma ALD process ABC* is optimized. From the SE measurements, saturation times of 8 s, 5 s and 0.5 s are required for step A, B and C respectively. According to OES data, plasma exposure times of at least 5 s $O_2$ plasma and 2.5 s $H_2$ plasma must be chosen. Results of SE and OES measurements during the $O_2$ plasma exposure are in agreement. Comparison of the OES and SE results of the hydrogen step leads to different required $H_2$ plasma exposures times. The reason could be that, after 0.5 s exposure, the reduction reaction is completed and the growth rate is constant, but the reaction product are still in the reactor. After 2.5 s when the plasma exposure starts, the last reaction products dissociate and only background emission is measured. Further research in the reaction mechanism and the detection of the reaction products by OES should prove that this could be the reason. In the optimized process, presented in Table 4.1, 2.5 s $H_2$ plasma exposure is chosen, for ensuring the reduction reaction is completed. The growth rate saturates to $\sim$0.42 $\pm$ 0.02 Å/cycle for the three saturation curves of process ABC*. This is consistent with the growth rate of $\sim$0.40 $\pm$ 0.04 Å/cycle measured on the ALD-I setup.

*Table 4.1:* Optimized ABC* process for Pt ALD at room temperature, based on SE and OES measurements. The final pressure of the Ar (50 sccm) and precursor gas during the precursor dosing is about 9.5 mTorr, whereas the butterfly valve was put under an angle of 35°. During the Ar purge, the butterfly valve was fully open (90°). The gases $O_2$ and $H_2$ (and their plasmas) were set to a pressure of 12 mTorr controlled by setting the butterfly valve at 30°. Pump times are chosen sufficiently long but can also be optimized with further research.

| Precursor step | Pump down | $O_2$ reactant step 50 sccm | Pump down | $H_2$ reactant step 50 sccm | Pump down |
|---|---|---|---|---|---|
| 1 s Ar 50 sccm<br>8 s $MeCpPtMe_3$ dosing with 50 sccm Ar<br>3 s Ar purge 100 sccm | 3 s | 3 s $O_2$ gas<br>5 s $O_2$ plasma<br>1 s $O_2$ gas | 3 s | 3 s $H_2$ gas<br>2.5 s $H_2$ plasma<br>1 s $H_2$ gas | 10 s |

Furthermore, there are little to none experiments done in this study for optimizing other elements of the process like i.e. pump times. Research with other pump times with SE and OES measurements could optimize the process further.

## 4.2 Comparison between Pt ALD at FlexAL and ALD-I setups

The main goal of this project is to optimize Pt ALD at the FlexAL setup. The optimized processes are listed in Table 3.1 and Table 4.1. Results of nucleation behavior of thermal ALD at the two setups are shown in Figure 4.1, which also includes the results of

Mackus [1] obtained at the ALD-I. The Figure shows that the nucleation behavior of Pt

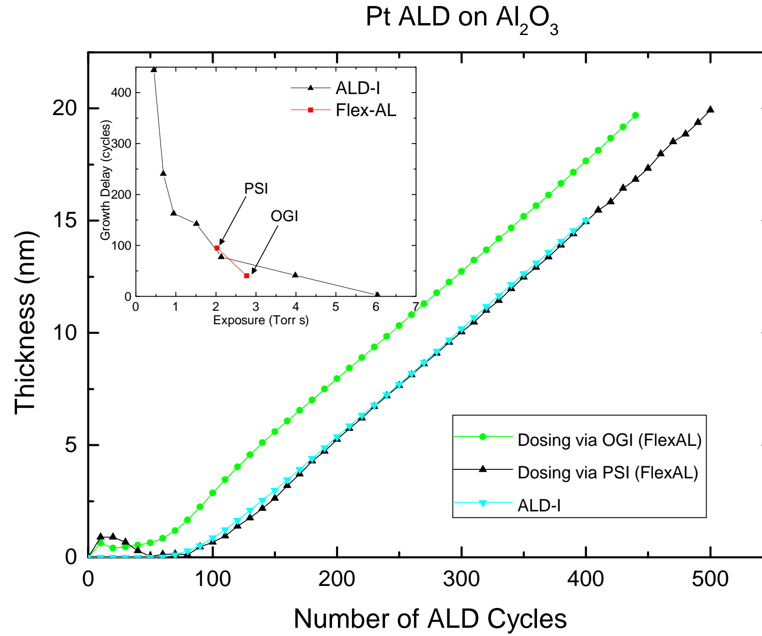


*Figure 4.1:* Nucleation curves showing the thickness as a function of the number of ALD cycles measured by *in situ* spectroscopic ellipsometry on $Al_2O_3$ substrates. For all processes on the FlexAL, it concern a thermal ALD process with 8 s $MeCpPtMe_3$ dosing and 10 s 300 mTorr $O_2$ dosing. Dosing at the FlexAL is done via the inlets of the ozone generator (OGI) or the plasma source inlet (PSI). Data from experiments of Mackus, which includes 3 s $MeCpPtMe_3$ dosing with 10 s oxygen dosing at the ALD-I setup, are also added. The oxygen dosing and pressure at the ALD-I are controlled by a mass flow controller. In the inset, the growth delay as function of the exposure at the FlexAL and ALD-I setup are shown.

ALD in the ALD-I follows the same trend as the behavior in the FlexAL setup when using dosing via the PSI. They have practically the same growth rate and nucleation delay. This is caused by the fact that the pressure evolution for these measurement are largely the same which results in about equal exposures. This is confirmed in the inset of Figure 4.1. From the inset it becomes clear that the growth delays are almost the same for the 300 mTorr measurements, in which the exposure for the FlexAL (for dosing via the PSI) and ALD-I is about 2 Torr s and the growth rates are 100 and 77.4 cycles, respectively. The nucleation behavior (with dosing via the OGI) has the same growth rate but has a smaller growth delay. This is caused by the fact that dosing via the OGI gives a larger exposure and has therefore a lower growth rate which is also confirmed from the inset. The pressure evolution for dosing via the OGI follows more a block pulse while dosing via the PSI (and ALD-I) has a gradual pressure evolution which is in accordance with the inset of Figure 4.1.

Furthermore, there is a big difference between the required duration of the precursor dosing to obtain saturation. Mackus used a process with 3 s precursor dosing for both thermal ALD and plasma ALD at room temperature. The required precursor dosing

time at the FlexAL is 8 s, for saturated ALD growth. Processes at the two setups consists of the same steps as can be seen in the tables. The difference in precursor dosing time is mainly caused by differences between the reactors which are shown in Table 4.2. Besides that all reactions must be in saturation, efficiently precursor dosing is also important for the optimization. It is plausible that the high precursor use at the FlexAL is caused by the large heated area which is about five times larger than the heated area of the ALD-I. Deposition mainly takes place at the heated substrate table. However, the substrate heater can radiative heat the walls to a temperature at which Pt growth could occur, and therefore, it was difficult to accurately estimate the total surface area on which Pt was actually deposited. The surface where deposition takes place is only based on the area of the substrate heater and other areas are neglected. Furthermore, the precursor temperature differs, namely 40°C at the FlexAL and 30°C at the ALD-I. A higher precursor temperature leads to higher precursor pressures which also lead to a higher use. Therefore, the difference in precursor consumption is caused by the difference in dosing times but also by the difference in precursor temperature. An

*Table 4.2:* Comparison between the ALD-I and FlexAL setup.

| **Parameter** | **ALD-I setup** | **FlexAL setup** |
|---|---|---|
| Temperature precursor | 30°C | 40°C |
| Ar flow | 0.01 mbar | 0.01 mbar/50sccm |
| Wall temperature | 80°C | 120°C |
| Butterfly valve | No | Yes |
| Substrate diameter | 100 nm | 200 mm |
| Substrate heater diameter | 102 mm | 240 mm |
| Surface area for deposition | 82 $cm^2$ | 398 $cm^2$ |
| Volume of chamber [14, 15] | (8.69±0.01) L | (21±1) L |

additional drawback is that the precursor $MeCpPtMe_3$ is very expensive. It is advisable to do Pt deposition at the ALDI-I instead of the FlexAL setup because of the high precursor consumption. However, for specific depositions on larger substrates or multilayer depositions, it could be useful to perform Pt deposition at the FlexAL setup.

# 5 Conclusion

In this study, thermal Pt ALD as well plasma Pt ALD were optimized on the FlexAL setup. The optimized thermal ALD process at 300°C comprises of 8 s $MeCpPtMe_3$ dosing and 10 s (300 mTorr) $O_2$ dosing. Nucleation curves show growth delays of 40 cycles and 95 cycles for respectively $O_2$ dosing via the OGI and PSI, which was caused by a difference in exposure. The optimized process leads to saturated ALD growth with a growth rate of ∼0.49 ± 0.02 Å/cycle which is consistent with results reported for the ALD-I setup (∼0.50 ± 0.01 Å/cycle [1]).

Deposition of Pt at room temperature was achieved with the optimized plasma ALD process ABC* which includes 8 s $MeCpPtMe_3$ dosing, 5 s $O_2$ plasma and 2.5 s $H_2$ plasma exposure. The optimization is based on SE and OES measurements and a growth rate of ∼0.42 ± 0.02 Å/cycle was measured, which is also consistent with the measured growth rate on the ALD-I setup (∼0.40 ± 0.04 Å/cycle [1]). From time-resolved OES measurements, it becomes clear that $H_\alpha$ and OH are an indication for the occurrence of combustion reactions during the $O_2$ plasma step and reduction reactions during the $H_2$ plasma step.

Comparison to the results on the ALD-I setup has led to the conclusion that the precursor consumption is relatively high for depositions on the FlexAL setup. This is probably caused by the difference in heated surface area where deposition takes place which is much larger in the FlexAL. Wafers up to 200 mm can be handled at the FlexAL which has therefore a five times larger table surface heater than the ALD-I (which handles wafers up to 100 mm). This larger surface causes a high precursor consumption. An additional disadvantage is that MeCpPtMe3 is an expensive precursor. A recommendation is, mainly from a cost perspective, to perform Pt ALD on the ALD-I setup. However, for specific depositions on large substrates or multi-layer depositions, it could be useful to perform Pt deposition at the FlexAL setup.

# 6 Outlook

Several conclusions have been drawn in this report. However, some questions remain unanswered. This outlook is given to show which elements still require attention. Based on the results of this report, the following recommendations for further research can be given:

- Optimization of precursor consumption by varying the butterfly valve. Besides measuring the saturation curves in this report, also a few experiments were performed with different pressures during the argon and precursor steps. The pressures were varied by setting the butterfly valve at different angles. An angle of 35° was the standard condition in the experiments described in section 2.2. Putting the angle at 10°, leads to an almost closed valve which results in a long residence time of the gas species and, a high chamber pressure. Pressures in the range of 100 mTorr to 170 mTorr occurred which are much higher than the set pressure of 9.5 mTorr that is used in experiment of this report. The saturation measurements, with the butterfly valve at 10°, leads to higher growth rates (∼0.53 - 0.55 Å/cycle) as expected (see Figure A.1). These high growth rates cannot be explained by theory. A maximum growth rate of about ∼0.50 ± 0.01 Å/cycle was expected. The effect is also seen with low oxygen pressure (10 mTorr) for which a growth rate per cycle of 0.45 ± 0.04 Å/cycle is expected [1] and ∼0.48 ± 0.01 Å/cycle was measured (see Figure A.2). The high growth rates could be taken as starting point for further research with varying the butterfly angles.

- In section 3.1.2, momentarily higher growth rates were measured before the growth rate became constant. The higher growth rates are probably caused by island growth which is typically for Pt growth on $Al_2O_3$ substrates. At some point, the islands have a larger surface area than a continuous, straight film. However it is very difficult to investigate the islands shape simply by measuring it. In order to be able to say more about the island growth, simulations for ALD growth on different island shapes could be achieved. From comparison of the nucleation behavior from the experiment and the simulations, more details about the Pt island shapes can be concluded.

- Further optimization of the ABC* process by varying the pump times. The optimized process is mentioned in Table 4.1. However, duration of the pump times are not optimized and it is likely that these times can be reduced.

- More insight in the OES data. Several OES measurements are done and (time-resolved) spectra are discussed in this report. However, more insight in the OES data could lead to better understanding of the reaction mechanism. For example, no $CO_2$ and CO emission (Ångström and Herzberg systems) was measured during the $O_2$ plasma exposure while $CO_2$ is supposed to be a reaction product.

# References


[1] A.J.M. Mackus. *Atomic layer deposition of platinum: from surface reactions to nanopatterning*. PhD thesis, Eindhoven University of Technology, 2013.

[2] H.B. Profijt. *Plasma-surface interaction in plasma-assisted atomic layer deposition*. PhD thesis, Eindhoven University of Technology, 2012.

[3] T. Aaltonen, A. Rahtu, M. Ritala, and M. Leskelä. Reaction mechanism studies on atomic layer deposition of ruthenium and platinum. *Electrochem. Solid State Lett.*, 6:C130, 2003.

[4] Francisco Zaera and Helmuth Hoffmann. Detection of Chemisorbed Methyl and Methylene Groups: Surface Chemistry of Methyl Iodide on Pt(ll1). *J. Phys. Chem. C*, 95:6297, 1991.

[5] Francisco Zaera. Study of the surface chemistry of methyl iodide coadsorbed with hydrogen on Pt(111). *Surf. Sci.*, 262:335, 1992.

[6] W. M. M. Kessels, H. C. M. Knoops, S. A. F. Dielissen, A. J. M. Mackus, and M. C. M. van de Sanden. Surface reactions during atomic layer deposition of Pt derived from gas phase infrared spectroscopy. *Applied Physics Letters*, 95:013114, 2009.

[7] H.B. Profijt, S.E. Potts, M.C.M. van de Sanden, and W.M.M. Kessels. Plasma-assisted atomic layer deposition: Basics, opportunities, and challenges. *Journal of Applied Physics*, 29:FE0000, 2011.

[8] E.M.J. Braeken. Development and understanding of a plasma-assisted atomic layer deposition process for silicon nitride. Master Thesis, 2013.

[9] N.F.W. Thissen. Nucleation of platinum during Atomic Layer Deposition as studied by Spectroscopic Ellipsometry and Transmission electron microscopy. Bachelor End Project, 2010.

[10] E. Langereis, S.B.S. Heil, H.C.M. Knoops, W. Keuning, M.C.M. van de Sanden, and Kessels W.M.M. In situ spectroscopic ellipsometry as a versatile tool for studying atomic layer deposition. *Journal of Applied Physics D-applied Physics*, 42:073001, 2009.

[11] A.J.M. Mackus, S.B.S. Heil, E. Langereis, H.C.M. Knoops, M.C.M. van de Sanden, and Kessels W.M.M. Optical emission spectroscopy as a tool for studying, optimizing and monitoring plasma-assisted atomic layer deposition processes. *Journal of Vacuum Science and Technology A*, 28:77, 2010.

[12] R. Vervuurt. Nucleation curve of Pt ALD on $Al_2O_3$. private communication, 2013.

[13] R.L. Puurunen and W. Vandervorst. Island growth as a growth mode in atomic layer deposition: A phenomenological model. *Journal of Applied Physics*, 96:7686, 2004.

[14] N. Leick, S. Agarwal, A.J.M. Mackus, S.E. Potts, and W.M.M. Kessels. Catalytic Combustion Reactions During Atomic Layer Deposition of Ru Studied Using $^{18}O_2$ Isotope Labeling. *J. Phys. Chem. C*, 117:21320, 2013.

[15] S.A.F. Dielissen. Atomic layer deposition of platinum studied by gas phase infrared spectroscopy. Bachelor End Project, 2008.

# A Appendix

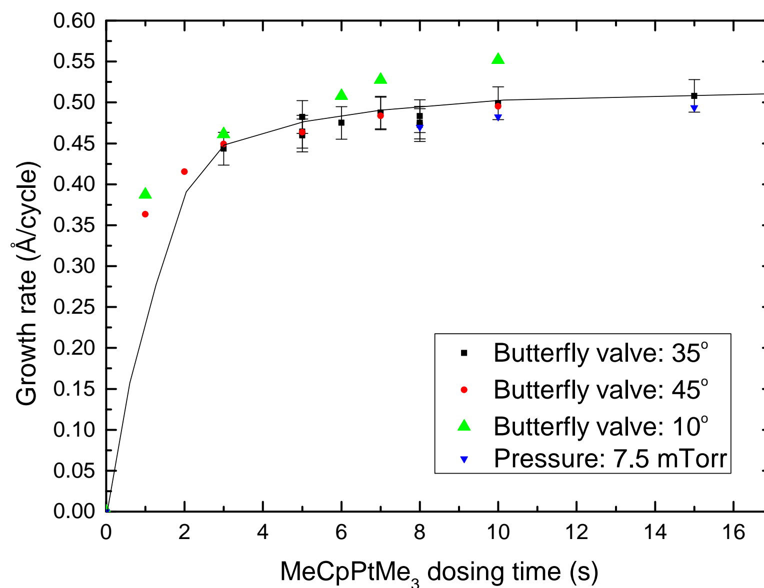


*Figure A.1:* The growth rate as a function of the $MeCpPtMe_3$ dosing time, as measured by *in situ* spectroscopic ellipsometry. The pressure in the precursor step is controlled by setting the butterfly valve at different angels or by setting the pressure in the APC at 7.5 mTorr. It concerns a thermal ALD process with 10 s 300 mTorr (50 sccm) $O_2$ dosing (via the plasma source inlet). The black line serves as a guide to the eye.

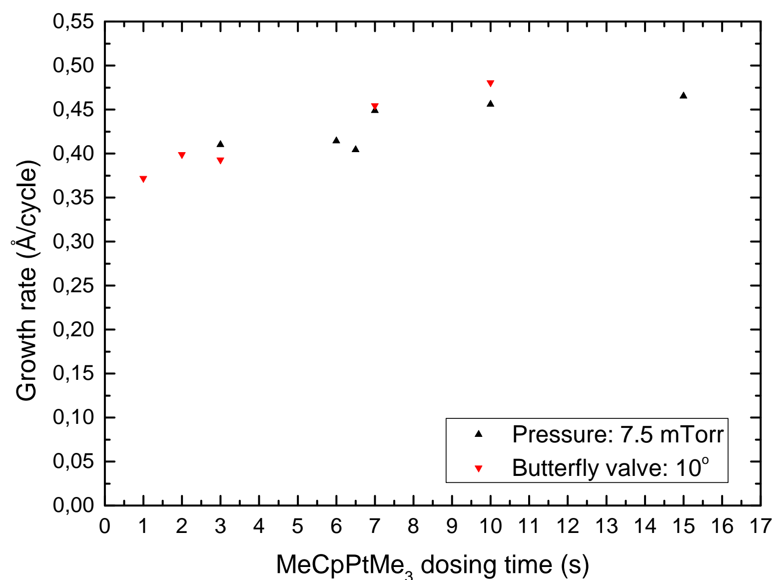


*Figure A.2:* The growth rate as a function of the $MeCpPtMe_3$ dosing time, as measured by *in situ* spectroscopic ellipsometry. The pressure in the precursor step is controlled by setting the butterfly valve at 10° or by setting the pressure in the APC at 7.5 mTorr. It concerns a thermal ALD process with 10 s (50 sccm) $O_2$ dosing (via the plasma source inlet). The oxygen pressure is about 10mTorr and is controlled with the butterfly at 30°